

3D mode shape visualization system based on laser

レーザスペckルを利用した3次元振動変位可視化システム

Yuichiro Yano[†], Yasuaki Watanabe, Shigeyoshi Goka, Takayuki Sato and
Hitoshi Sekimoto (Grad. School of Sci. and Eng., Tokyo Metropolitan Univ.)

矢野 雄一郎[†], 渡部 泰明, 五箇 繁善, 佐藤 隆幸, 関本 仁 (首都大院)

1. Introduction

Piezoelectric resonators, in particular quartz resonators, are widely used in electronic devices such as mobile phones. Recent advances in computer technology have enabled the application of finite element analysis to the design of piezoelectric resonators, and confirming the reliability of the calculated results is very important when designing such resonators. Comparing the mode shape predicted by analysis with the shape obtained experimentally is the best way to obtain positive proof of the design reliability. For this reason, a number of methods for plotting the vibration patterns of piezoelectric resonators have been developed and reported [1–16].

We have now developed an improved system for visualizing the 3-D vibration modes on the device surface in quasi-real time without the need for precise optical adjustment. Three visible wavelength semiconductor lasers with adequately separated wavelengths are used, and their incident angles are set to detect the two in-plane vibrations and one out-of-plane vibration. A color video camera using three CCDs (red, green, and blue) captures the three isolated speckle images generated by each laser. To reduce image noise and calculation time, we developed an enhanced two-dimensional correlation filter. Testing using AT-cut quartz resonators demonstrated the effectiveness of this improved system.

2. Measurement Principle

The surface vibration displacement of piezoelectric resonators can be decomposed into two in-plane (u_1 and u_3) components and one out-of-plane (u_2) component. These vibration components can be separately measured by changing the incident angles of the coherent light sources (e.g., semiconductor lasers) [17].

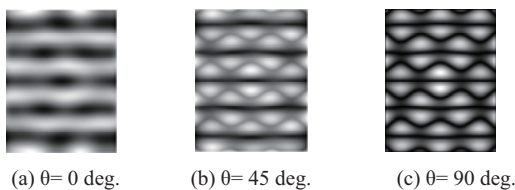


Fig. 1. Interference images calculated on basis of laser incident angle

Figures 1(a)–(c) show interference images calculated on the basis of the laser incidence angle for a fundamental thickness mode in a rectangular AT-cut quartz. The maximum magnitudes of the in-plane and out-of-plane vibration amplitudes at the resonator surface were approximately the same. In the images, the variation in the interference magnitude is expressed as an absolute value: the white regions represent areas of large vibration, and the black regions represent areas of small vibration. At angles of 0 and 90° (1(a) and (c)), the vibration components were unaffected by each other.

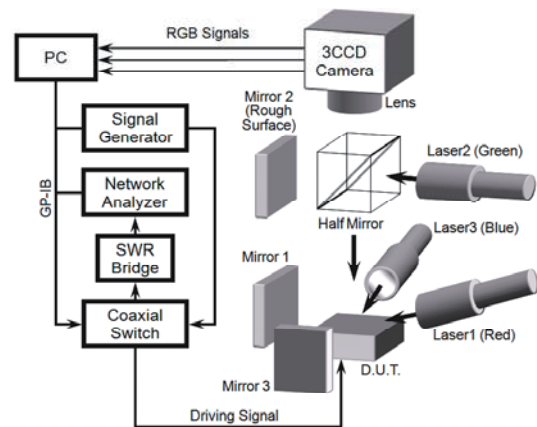


Fig. 2. Block diagram of measurement system

Figure 2 shows a block diagram of the measurement system. The resonator was driven by a signal generator (SG), and the driving signal was tuned to the resonant frequency. We used a frequency-shift technique to control the resonator driving state because the speckle patterns for the resonator driving and non-driving states are required for reconstituting the vibration modes. This technique enables software control of the resonator state without having to use an external control device.

The three lasers, which had linear polarization, generated visible-wavelength beams; the optical wavelengths and powers were 655 nm and 10 mW for the red laser, 405 nm and 30 mW for the violet laser, and 532 nm and 1 mW for the green laser. Optical diffusers inserted between the lasers and collimator lenses produced homogeneous scattering on the sample surface.

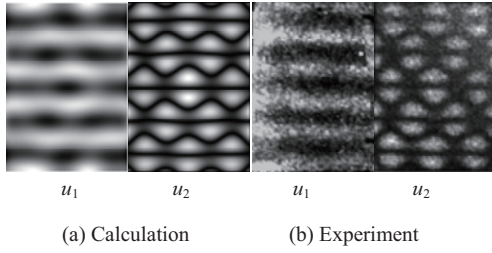


Fig. 3 Calculated and experimental results for TS-1 mode with rectangular AT-cut resonator: (a) calculation, (b) experiment.

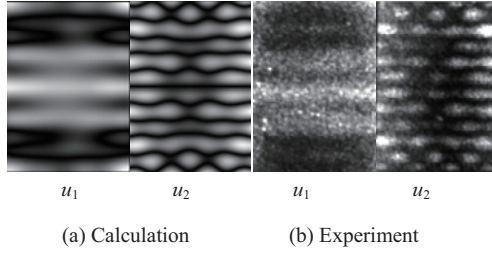


Fig. 4 Calculated and experimental results for inharmonic mode with rectangular AT-cut resonator: (a) calculation, (b) experiment.

3. Evaluation

To evaluate the feasibility of the proposed system, we applied it to the fundamental thickness shear mode and the inharmonic mode of a rectangular 1-MHz AT-cut quartz resonator. The dimensions of the resonator plate were $x_1(x) = 13.964$ mm, $x_2(y') = 1.737$ mm, and $x_3(z') = 10.000$ mm, and the standard deviation of the resonator surface roughness was $5.5 \mu\text{m}$. The ratio of the maximum displacements between the in-plane (u_1) and out-of-plane (u_2) vibrations was 0.7 from finite element analysis. We did not measure the u_3 component because its amplitude is negligible compared to those of the other two components due to the nature of an AT-cut quartz resonator.

One hundred pairs of images were accumulated for each speckle image, which took 12 sec. including the correlation calculation when the spatial resolution of the images was 640×480 pixels. Even faster measurement can be achieved by reducing the spatial resolution and the number of image pairs.

Figures 3(a) and (b) respectively show calculated [17] and experimental results for full-field motion of the fundamental thickness shear (TS-1) mode. The left image of each pair shows the mode shape for in-plane (u_1) vibration, and the right one shows that for out-of-plane (u_2) vibration. Again, the amplitude of the vibration displacement is expressed as an absolute value; that is, the white regions represent areas of large displacement, and the black regions represent areas of small displacement.

The experimental results correspond well to the calculated images on the left. This shows that the proposed system estimates both the u_1 and u_2 components of the vibration displacement well.

Figures 4(a) and (b) show calculated and experimental results for full-field motion of the inharmonic mode near the fundamental mode. Again, the proposed system estimated both the u_1 and u_2 components of the vibration displacement well.

4. Conclusion

We have developed a 3D-mode shape visualization system that uses a laser speckle interferometer, a color video camera with three CCDs.

Since the frequency range of the proposed system is limited only by that of the RF-generator that excites the device under test, the system can be applied to ultra-high frequency devices such as MEMS devices operating in the GHz range.

Acknowledgment

This work was partially supported by Grant-in-Aid for Scientific Research (C), No.20560399, from the Ministry of Education, Culture, Sports, Science and Technology, Japan.

References

- [1] R. J. Williamson: Proc. 44th Annu. Symp. Freq. Control, 1990, pp. 424.
- [2] H. J. Tizianni: Optica Acta **18** (1971) 891.
- [3] D. E. Duffy: Appl. Opt. **11** (1972) 1778.
- [4] J. Monchalin: IEEE Trans. Ultrason. Ferroelectr. and Freq. Control **35** (1986) 485.
- [5] W. Wang, C. Hwang and S. Lin: Appl. Opt. **35** (1996) 4502.
- [6] C. Ma and C. Huang: IEEE Trans. Ultrason. Ferroelectr. and Freq. Control **48** (2001) 142.
- [7] Y. Watanabe, Y. Shikama, S. Goka, T. Sato and H. Sekimoto: Jpn. J. Appl. Phys. **40** (2001) 3572.
- [8] Y. Watanabe, T. Tominaga, T. Sato, S. Goka and H. Sekimoto: Jpn. J. Appl. Phys. **41** (2002) 3313.
- [9] Y. Watanabe, T. Sato, S. Goka and H. Sekimoto: Proc. IEEE Ultrasonic Symp., 2002, pp. 928.
- [10] Y. Watanabe, S. Goka, T. Sato and H. Sekimoto: IEEE Trans. Ultrason. Ferroelectr. and Freq. Control **51** (2004) 491.
- [11] Y. Watanabe, K. Tsuno, T. Tsuda, S. Goka, T. Sato and H. Sekimoto: Proc. 2004 Annu. Symp. Freq. Control, 2004, pp. 591.
- [12] Y. Watanabe, K. Tsuno, T. Tsuda, S. Goka and H. Sekimoto: Jpn. J. Appl. Phys. **44** (2005) 4440.
- [13] Y. Watanabe, T. Tsuda, S. Ishii, S. Goka and H. Sekimoto: Jpn. J. Appl. Phys. **45** (2006) 4585.
- [14] Y. Watanabe, S. Ishii, S. Goka, H. Sekimoto, M. Kato and T. Tsuda: Proc. 2006 Annu. Symp. Freq. Control, 2006, pp.554
- [15] Y. Watanabe, N. Imaeda, S. Ishii, S. Goka, T. Sato and H. Sekimoto: Proc. 2007 Annu. Symp. Freq. Control, 2007, pp.160-163.
- [16] K. Tachibana, Y. Watanabe, N. Imaeda, S. Goka, T. Sato, and H. Sekimoto: Jpn. J. Appl. Phys. **48** (2009) 07GC04
- [17] Y. Watanabe, T. Sato, S. Goka and H. Sekimoto: Acoust. Sci. & Tech. **23** (2002) 284.